



2 Assessment of composite global sampling: Sea surface wind speed

3 Huai-Min Zhang,¹ John J. Bates,¹ and Richard W. Reynolds¹

4 Received 5 June 2006; revised 20 July 2006; accepted 10 August 2006; published XX Month 2006.

6 [1] Research and forecasts of the weather-ocean-climate
7 system demand increasingly higher resolution forcing data.
8 Here we assess the improvement in composite global
9 observations and the feasibility of producing high
10 resolution blended sea winds. The number of the long-
11 term US sea surface wind speed observing satellites has
12 increased from one in July 1987 to five or more since
13 2000. Global 0.25° gridded, blended products with
14 temporal resolutions of 6-hours, 12-hours and daily have
15 become feasible since mid 2002, mid 1995 and January
16 1991, respectively (with $\geq 75\%$ time coverage and $\geq 90\%$
17 spatial coverage between 65°S–65°N). If the coverage is
18 relaxed, the feasible times can be extended to earlier
19 periods. These statistics provide practical guidance to
20 produce reliable blended products for different
21 applications, and serve as guidance on the design of
22 future global observing systems. **Citation:** Zhang, H.-M.,
23 J. J. Bates, and R. W. Reynolds (2006), Assessment of composite
24 global sampling: Sea surface wind speed, *Geophys. Res. Lett.*, 33,
25 LXXXXX, doi:10.1029/2006GL027086.

27 1. Introduction

28 [2] The Earth's weather and climate system is driven by
29 two major constantly changing components – the atmo-
30 sphere and the ocean. These two components vigorously
31 interact with each other over about 70% of the Earth's
32 surface and these interactions directly regulate the Earth's
33 water and energy cycles. Advances in understanding this
34 coupled system and improvements in numerical weather
35 and ocean forecasts demand increasingly higher resolution
36 data on wind and air-sea fluxes, as documented in several
37 World Meteorology Organization (WMO) programs [e.g.,
38 *World Meteorological Organization*, 2000; *Curry et al.*,
39 2004] [also *Large et al.*, 1991]. Some of the applications
40 require temporal and spatial resolutions of up to 3 hours and
41 50 km. However, to what extent these requirements can be
42 met in reality by the existing global observing system of
43 multiple satellites and in-situ observations has not been
44 systematically studied. In this work we seek to answer this
45 question for sea wind speed, a dominant parameter in
46 forcing numerical models and in determining the turbulent
47 air-sea fluxes [e.g., *Fairall et al.*, 2003].

48 [3] The composite statistics will be presented in the
49 following sections with increasing complexity, and the
50 results and discussion of one section will serve as the foun-
51 dation for the next section. Section 2 describes the available
52 sea wind observations. Section 3 presents a case study of the

composite sampling in a day. Section 4 extends the composite 53
analysis to the whole sea-wind satellite era in terms 54
of averaged sampling time intervals. Section 5 examines 55
the spatial and temporal data coverage for specific temporal 56
resolutions. Lastly, section 6 features the summary and 57
discussion. 58

2. Sea Surface Wind Speed Observations 59

[4] Sea surface wind has been traditionally observed 60
from in-situ platforms such as ships and buoys [e.g., 61
Bourassa et al., 2005; *Worley et al.*, 2005]. However, even 62
today in-situ observations still have very limited spatial 63
coverage over the vast ocean surface. Sea surface wind 64
speed has also been operationally observed from satellite 65
sensors, starting with a US Defense Meteorological Satellite 66
Program (DMSP) satellite F08 in July 1987 to the constel- 67
lation of 5 or more US satellites since 2000. In this satellite 68
era, in-situ observations still play a critical role in calibrating 69
and validating satellite observations. However, with the 70
dense satellite sampling, in-situ observations play a minor 71
role in reducing random and sampling errors in blended 72
analyses using in-situ and satellite observations [e.g., *Zhang* 73
et al., 2006]. Thus in this data sampling study, we only 74
consider satellite observations. 75

[5] The time line of the long-term US sea surface wind 76
speed observing satellites is shown in Figure 1. Note that in 77
this long-term assessment study, we have not used the short- 78
lived wind satellites (e.g., the US National Aeronautics and 79
Space Agency Scatterometer (NSCAT), the joint US/Japan 80
SeaWinds on the Advanced Earth Observing Satellites 81
(ADEOS) I & II), non-US satellites (e.g., the European 82
Remote Sensing Satellites (ERS) –1 and 2, which have 83
narrow observing swaths and interrupted observations), and 84
satellites from which sea surface wind speed can also be 85
retrieved (presently with less accuracy) along with the 86
primary product of sea level (e.g., the joint US/French 87
altimetry satellites of Ocean Topography Experiment 88
(TOPEX)/Poseidon and the follow-on Jason). Inclusion of 89
these data would have limited positive impact for the 90
corresponding time periods on this sampling study. 91

[6] Among the satellites in Figure 1, the passive DMSP 92
observations are from the microwave radiometers on the 93
Special Sensor Microwave Imager (SSM/I [*Hollinger et al.*, 94
1987; *Wentz*, 1997]). Later additions to these passive 95
microwave observations are the Tropical Rainfall Measuring 96
Mission (TRMM) Microwave Imager (TMI [*Kummerow et al.* 97
et al., 1998]) and the Advanced Microwave Scanning Radio- 98
meter of NASA's Earth Observing System (AMSR-E 99
[e.g., *Wentz and Meissner*, 1999]). The scatterometer 100
(e.g., the Quick Scatterometer (QuikSCAT)), which is 101
active by nature, uses microwave radar and retrieves both 102
wind speed and wind direction [e.g., *Dunbar et al.*, 1991a, 103
1991b; *Liu et al.*, 1998]. 104

¹National Climatic Data Center, NOAA NESDIS, Asheville, North Carolina, USA.

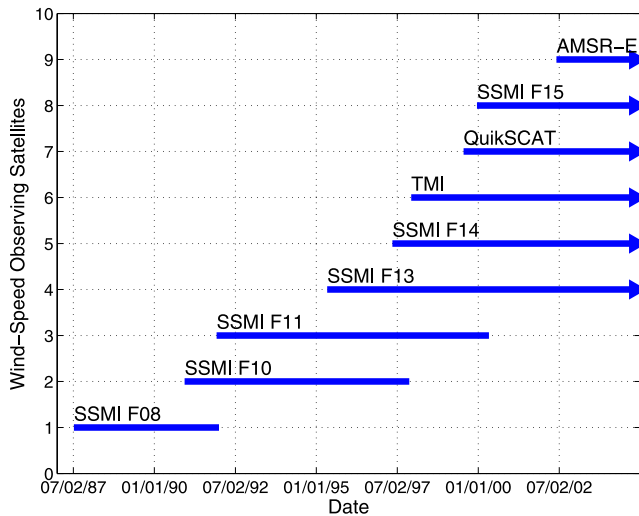


Figure 1. Timeline of the long-term US sea surface wind speed satellites used in this study.

[7] In the following we quantify the temporal improvement of the composite global data sampling rate from the satellites shown in Figure 1. The individual satellite data were obtained from the Remote Sensing Systems (RSS), Inc. [e.g., *Wentz, 1997*]. The RSS data were chosen for their uniformity of the retrieval algorithms for the multiple satellites over the whole time period, and for their wide use in producing various air-sea turbulent fluxes [e.g., *Chou et al., 2003*, and references therein]. Using these datasets, we explore the possibility of producing blended global products on a 0.25° global grid for various temporal resolutions. This 0.25° spatial grid marginally resolves ocean boundary currents such as the Gulf Stream where large turbulent fluxes and large flux gradients frequently occur. An improved daily sea surface temperature analysis is also produced on this spatial grid [*Reynolds et al., 2006*].

3. Daily Composite Global Sampling: A Case Study

[8] This section describes a case study to lay out the fundamental satellite observational information for the statistical analyses in the following sections. Figure 2 shows an example of the composite observations from the six satellites since mid 2002. The equator-crossing-times (ECTs) in Local Solar Time (LST) of the five polar-orbiting satellites (DMSP F13, F14, F15, QuikSCAT and AMSR-E) are typical for this time period, and the actual observation times in LST along individual tracks from the Equator to mid latitudes vary little, but change more rapidly in the Polar Regions (thus shown as long lines but not drawn near the Pole). In contrast, the ECTs of the equator-orbiting TMI satellite vary from day to day (shown for January 20) and the actual observation times also vary more rapidly even along a single track between roughly 40°N and 40°S (thus shown by short lines). Overall, the shown satellites are not evenly positioned around the Earth; however, with all the ascending and descending tracks, the observations span over the whole day fairly well with the additions of the TMI and AMSR-E.

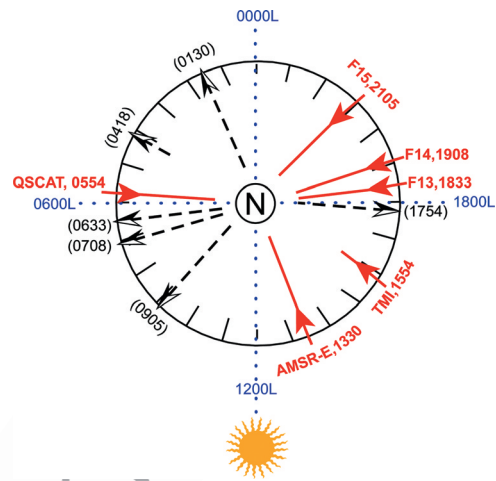


Figure 2. A simplified view looking down at the North Pole of the satellite observations in Local Solar Time (LST) of January 2005. Solid lines and arrows indicate ascending tracks and dashed lines and open arrows indicate descending tracks.

[9] The above is a quasi-Lagrangian view following the satellite tracks in local solar time. However, most gridded global products are generated as Eulerian fields on Earth, i.e. as global snapshots at specific Coordinated Universal Time (UTC) or as averages over certain UTC time periods. The Eulerian fields are required by many applications such as numerical modeling and computation of wind stress divergence or vorticity (when used together with wind directions). Figure 3 shows the distribution of the combined

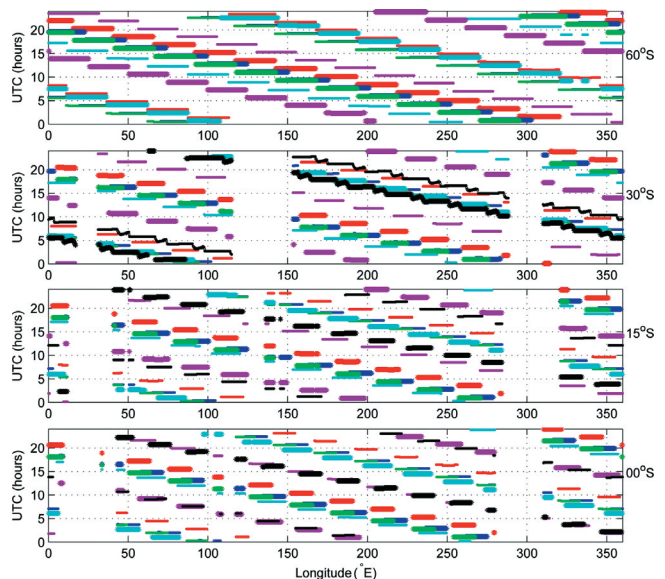


Figure 3. Oceanic satellite passing time (in UTC) along four latitude circles for 1 January 2005. Data bins are 0.25° by 0.25° in space. Top to bottom panels are for 60°S , 30°S , 15°S and the Equator, respectively. Thicker lines by '+' signs indicate ascending tracks and thinner lines by '.' signs indicate descending tracks. Each color represents one satellite: Red – F15, blue – F14, green – F13, black – TMI, cyan – QuikSCAT, and magenta – AMSR-E.

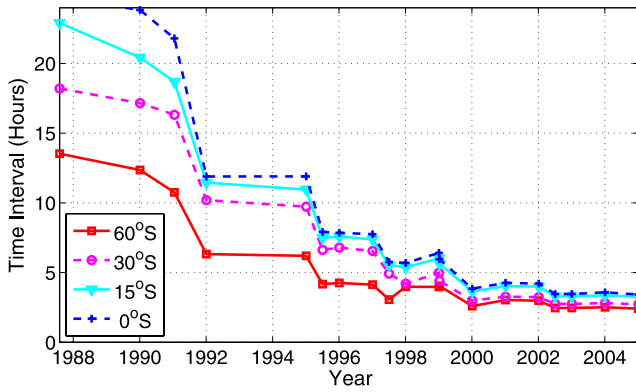


Figure 4. Averaged sampling time interval in the 0.25° bins, as functions of time and selected latitudes. Shown are averages along the individual latitude circles and over 1-week periods at the beginning of selected months, for which there were new satellite additions or reductions.

152 satellite observation times in UTC as functions of longitude
153 (x-axis) and latitude (top to bottom panels). Sampling
154 features in the Northern Hemisphere are similar but with
155 more land masses (shown as horizontal data gaps).

156 [10] On this date (1 January 2005) and in most areas of
157 the global ocean, the 0.25° bins are sampled multiple times
158 (about 9.9, 8.7, 7.3 and 6.9 times on zonal average at the
159 four latitudes) and the sampling times spread out over the
160 24-hour period fairly well although there are not strictly
161 uniform. The slanting structure reflects the paths of the
162 polar-orbiting satellites which result in a general sampling
163 increase with increasing latitude.

164 4. Temporal Improvement in Averaged 165 Sampling Time Intervals

166 [11] From Figure 3 and at fixed longitude and latitude,
167 differencing the adjacent observing times results in individ-
168 ual sampling time intervals:

$$\Delta t_i = t_{i+1} - t_i,$$

169 where i indicates the discrete time points. The sampling
171 time intervals are general not uniform in neither time nor
172 space (Figure 3); here we first present an averaged view in
173 Figure 4 (more detailed studies in sections to follow). The
174 averaged sampling time intervals generally decreased with
175 increasing latitudes (shown by the four curves). They also
176 decreased rapidly from late 1987 to mid 1990s, from more
177 than 14 hours to less than 8 hours. Further decreases from
178 the mid 1990s were more moderate and the tropics and high
179 latitudes eventually converged in early 2000, at which the
180 averaged time intervals decreased to less than 5 hours.

181 [12] The averaged views are only useful for relatively
182 uniform spacing of the data points (e.g., Figure 3). For
183 highly inhomogeneous data distribution (in either time or
184 space), the conclusion from this type of averaging may be
185 misleading, as easily seen from the formulation of the time
186 averaging:

$$\overline{\Delta t} = \frac{\Delta t_1 + \Delta t_2 + \dots + \Delta t_{N-1}}{N-1} = \frac{t_N - t_1}{N-1},$$

where the bar indicates the average between time t_N and t_1 .
187 The above average depends only on the two end points and
188 the total number of the observations, N . It does not depend
189 on how the data are distributed between the end points. A
190 worst hypothetical scenario would be that the six satellites
191 observe at the same time. In this case the actual sampling
192 resolution is more like $t_N - t_1$ rather than the averaged
193 sampling time interval $(t_N - t_1)/(N-1)$. Some other cases for
194 the scatterometer satellites have been discussed by *Schlack et*
195 *al.* [2001].
196
197

198 5. Data Coverage for Various Fixed Resolutions

199 [13] In this section we present detailed assessment of the
200 more realistic data coverage for the global 0.25° grid and
201 various temporal resolutions (6-hourly, 12-hourly and daily)
202 over the whole wind-satellite era. The first shown will be
203 the temporal percentage data coverage for fixed spatial and
204 temporal resolutions. Specifically, for each 0.25° grid box
205 and fixed temporal resolution (i.e., sampling time interval,
206 e.g., 6 hours), the percentage in time with data coverage
207 over a month was computed, as shown in Figure 5 for
208 January 2005 as an example. This picture is typical for the
209 time period since mid 2002 when the AMSR-E was added.
210 In the mid latitudes ($40^\circ\text{S} - 60^\circ\text{S}$ and $40^\circ\text{N} - 60^\circ\text{N}$), the vast
211 majority of the global 0.25° boxes are sampled nearly 100%
212 of the time within each 6-hour time window. The majority
213 of the 0.25° boxes in the low to mid latitudes ($40^\circ\text{S} - 40^\circ\text{N}$)
214 are also sampled more than 75% of the time. Overall, about
215 92% of the global 0.25° oceanic boxes between $65^\circ\text{S} - 65^\circ\text{N}$
216 are sampled 75% of the time or better within each 6-hour
217 time period.

218 [14] Different applications (e.g., studies on cyclones,
219 coastal ocean forecast, and global modeling) may have
220 different requirements on data coverage. The above tempo-
221 ral and spatial data coverage statistics were also computed
222 for other time periods and for the temporal resolutions of
223 6-hourly, 12-hourly and daily. The results are listed in Table 1
224 and will be summarized in the next section. In this table, the

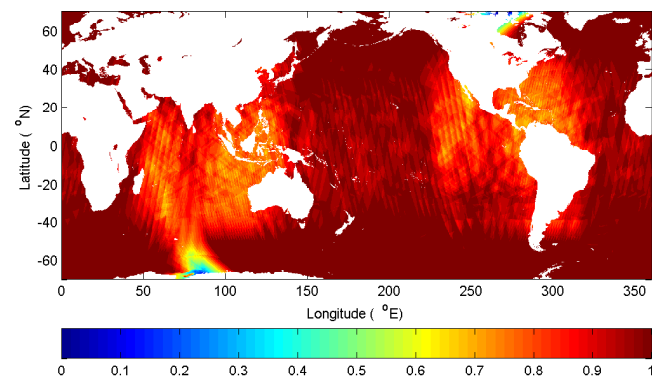


Figure 5. Temporal percentage of data availability within a month (January 2005) for a time interval of 6-hours (03Z – 09Z) and on the global 0.25° grid. Color scale 1 indicates data availability of 100% of the time.

t1.1 **Table 1.** Typical Percentages of the Global 0.25° Oceanic Boxes Between 65°S and 65°N In Which There Are Data Coverage 75% of the Time or Better for the Specified Time Resolutions and as Functions of Time^a

		Time Period and Satellite					
		JUL1987,	JAN1991,	JUN1995,	JAN1998,	JAN2000,	JUN2002,
Time	Resolution	I	II	III	IV	V	VI
		F08	F10, F11	F10, F11, F13	F11, F13, F14	F13, F14, F15	F13, F14, F15 TMI, QSCAT
					TMI	TMI, QSCAT	AMSR-E
t1.4	6-hourly	12	26	42	56	66	91
t1.5	12-hourly	27	72	97	99	100	100
t1.6	Daily	75	100	100	100	100	100

t1.7 ^aThe whole time period is classified into six stages corresponding to the typical number of available satellites. The time periods with $\geq 90\%$ spatial coverage and $\geq 75\%$ temporal coverage are bold.

225 sea-wind satellite era is classified into six time periods
 226 according to the number of available satellites and the
 227 resulting data coverage improvements. The listed spatial
 228 percentage coverage is for temporal percentage coverage of
 229 $\geq 75\%$ for each 0.25° grid box.

230 6. Summary and Discussion

232 [15] Research and forecasts of the weather-ocean-climate
 233 system demand increasingly higher resolution forcing data.
 234 In this paper, we assessed the feasibility of producing
 235 various high resolution blended products for sea surface
 236 wind speed from the existing global observing system.

237 [16] At the temporal resolution of daily (24 hours, bottom
 238 row in Table 1), one SSMI satellite in stage I provided data
 239 coverage over about 75% of the global 0.25° oceanic boxes
 240 between 65°S–65°N. Beginning with stage II when there
 241 were two or more satellites, the spatial coverage was
 242 increased to about 100%.

243 [17] At the temporal resolution of 12-hourly (2nd row
 244 from the bottom in Table 1), one satellite in stage I provided
 245 data coverage to less than 30% of the oceanic grid boxes.
 246 The addition of the second SSMI satellite in stage II
 247 drastically increased the spatial coverage to just below
 248 75%. Beginning with stage III when there were three or
 249 more satellites, the spatial coverage was increased to above
 250 95%.

251 [18] At the temporal resolution of 6-hourly (3rd row from
 252 the bottom in Table 1), the spatial coverage was less than
 253 30% with two or fewer satellites in stages I and II. In stage
 254 III, the coverage was about 42% with the three SSMI
 255 satellites (F10, F11 and F13). In stage IV, with the addition
 256 of the TMI, the spatial coverage increased to about 56%. In
 257 stage V, the addition of the QuikSCAT further increased the
 258 spatial coverage to about 66%. This modest increase is due
 259 to the close sampling times of the QuikSCAT and the SSMI
 260 satellites (Figure 2), although their ascending and descend-
 261 ing tracks are out-of-phase. However, in stage VI, the
 262 addition of the AMSR-E dramatically increased the spatial
 263 coverage to above 90%. The critical importance of the
 264 AMSR-E for high resolution products (6-hourly in this
 265 case) was also previously indicated by its unique sampling
 266 times compared to the other satellites (Figure 2).

267 [19] In conclusion, on the global 0.25° grid, blended
 268 products with temporal resolutions of 6-hours, 12-hours
 269 and daily have become feasible since mid 2002, mid 1995
 270 and January 1991, respectively (with $\geq 75\%$ time coverage
 271 and $\geq 90\%$ spatial coverage between 65°S–65°N). The
 272 corresponding feasible times can be farther extended back

to the beginning of 2000, beginning of 1991 and late 1987
 when the minimum spatial coverage was reduced to 65%,
 70% and 75%, respectively for the above three temporal
 resolutions.

[20] Lastly, we mention our available blended sea sur-
 face wind speed product. This product is based on the
 above statistics and for an initially uniform blending for the
 whole sea wind satellite era (July 1987 – present), thus a
 12-hourly time window was chosen. Sub-sampling aliases
 may still be large in this product for the early few years
 (Table 1). To take the advantage of the denser sampling in
 the latter years (especially since mid 2002), the blended data
 were generated 4 times a day at 00, 06, 12 and 18Z. To avoid
 heavy smoothing for the latter years with dense data, a
 Gaussian-like weighting function in both time and space
 was used to “penalize” data farther away from the inter-
 polation points [Zeng and Levy, 1995]. The gridded data and
 data production details are available at <http://www.ncdc.noaa.gov/oa/rsad/blendedseawinds.html>. Validation by in-situ data,
 data error analysis and intercomparisons with other products
 are subjects of future investigation.

[21] **Acknowledgments.** The individual satellite data were down-
 loaded from the website of the Remote Sensing System, Inc. (<http://www.remss.com/>). We thank Debra Smith (Remote Sensing System) for
 answering our detailed questions. Suggestions and critical comments from
 Ken Knapp and Lei Shi were a great help. Stimulating comments from two
 reviewers on an early version are greatly appreciated and enhanced the
 presentation. The views and findings in this report are those of the authors
 and should not be construed as an official NOAA or U.S. Government
 position, policy or decision.

References

- Bourassa, M. A., R. Romero, S. R. Smith, and J. J. O’Brien (2005), A new
 FSU winds climatology, *J. Clim.*, *18*, 3692–3704.
 Chou, S. H., E. Nelkin, J. Ardizzone, R. M. Atlas, and C. L. Shie (2003),
 Surface turbulent heat and momentum fluxes over global oceans based on
 the Goddard satellite retrievals, version 2 (GSSTF2), *J. Clim.*, *16*, 3256–
 3273.
 Curry, J. A., et al. (2004), SEAFUX, *Bull. Am. Meteorol. Soc.*, *85*(3),
 409–424.
 Dunbar, R. S., S. V. Hsiao, and B. H. Lambrigtsen (1991a), Science algo-
 rithm specifications for the NASA Scatterometer Project: Sensor Algo-
 rithms, *JPL D-5610-1*, Jet Propul. Lab., Pasadena, Calif.
 Dunbar, R. S., S. V. Hsiao, and B. H. Lambrigtsen (1991b), Science algo-
 rithm specifications for the NASA Scatterometer Project: Geophysical
 Algorithms, *JPL D-5610-2*, Jet Propul. Lab., Pasadena, Calif.
 Fairall, C. W., E. F. Bradley, J. E. Hare, A. A. Grachev, and J. B. Edson
 (2003), Bulk parameterization of air–sea fluxes: Updates and verification
 for the COARE algorithm, *J. Clim.*, *16*, 571–591.
 Hollinger, J., R. Lo, G. Poe, R. Savage, and J. Pierce (1987), Special Sensor
 Microwave/Imager’s user’s guide, technical report, 120 pp., Nav. Res.
 Lab., Washington, D. C.
 Kummerow, C., W. Barnes, T. Kozu, J. Shiue, and J. Simpson (1998), The
 Tropical Rainfall Measuring Mission (TRMM) sensor package, *J. Atmos.*

326	<i>Oceanic Technol.</i> , 15, 809–817.	
327	Large, W. G., W. R. Holland, and J. C. Evans (1991), Quasi-geostrophic	WCRP/SCOR Working Group on Air-Sea Fluxes (SCOR Working Group 344
328	response to real wind forcing: The effects of temporal smoothing, <i>J. Phys.</i>	110): Intercomparison and validation of ocean-atmosphere energy flux 345
329	<i>Oceanogr.</i> , 21, 998–1017.	fields, <i>WMO/TD-1036/WCRP-112</i> , 303 pp., Geneva. 346
330	Liu, W. T., W. Tang, and P. S. Polito (1998), NASA scatterometer provides	Worley, S. J., S. D. Woodruff, R. W. Reynolds, S. J. Lubker, and N. Lott 347
331	global ocean-surface wind fields with more structures than numerical	(2005), ICOADS release 2.1 data and products, <i>Int. J. Climatol.</i> , 25, 348
332	weather prediction, <i>Geophys. Res. Lett.</i> , 25(6), 761–764.	823–842. 349
333	Reynolds, R. W., K. S. Casey, T. M. Smith, D. B. Chelton (2006), A daily	Zeng, L., and G. Levy (1995), Space and time aliasing structure in monthly 350
334	blended analysis for sea surface temperature, paper presented at 86th	mean polar orbiting satellite data, <i>J. Geophys. Res.</i> , 100(D3), 5133– 351
335	AMS Annual Meeting, Am. Meteorol. Soc., Boston, Mass.	5142. 352
336	Schlag, M. G., D. B. Chelton, and M. H. Freilich (2001), Sampling errors in	Zhang, H.-M., R. W. Reynolds, and T. M. Smith (2006), Adequacy of the in 353
337	wind fields constructed from single and tandem scatterometer datasets,	situ observing system in the satellite era for climate SST, <i>J. Atmos.</i> 354
338	<i>J. Atmos. Oceanic Technol.</i> , 18, 1014–1036.	<i>Oceanic Technol.</i> , 23, 107–120. 355
339	Wentz, F. J. (1997), A well-calibrated ocean algorithm for SSM/I, <i>J. Geo-</i>	
340	<i>phys. Res.</i> , 102(C4), 8703–8718.	
341	Wentz, F. J., and T. Meissner (1999), AMSR Ocean Algorithm, version 2,	J. J. Bates, R. W. Reynolds, and H.-M. Zhang, National Climatic Data 356
342	<i>Tech. Rep. 121599a</i> , Remote Sens. Syst., Santa Rosa, Calif.	Center, NOAA NESDIS, 151 Patton Avenue, Asheville, NC 28801, USA. 358
343	World Meteorological Organization (2000), Final report of the Joint	(huai-min.zhang@noaa.gov) 359

Article in Progress